The 5th European sCO2 Conference for Energy Systems
March 14-16, 2023, Prague, Czech Republic

2023-sCO2.eu-116

# PERFORMANCE AND COST POTENTIAL FOR DIRECT-FIRED SUPERCRITICAL $CO_2$ NATURAL GAS POWER PLANTS

**Sandeep R Pidaparti**
National Energy Technology Laboratory/NETL
Support Contractor
Pittsburgh, USA

**Charles W. White**
National Energy Technology Laboratory/NETL
Support Contractor
Fairfax, USA

**Eric Liese***
National Energy Technology Laboratory
Morgantown, USA
Eric.Liese@netl.doe.gov

**Nathan T. Weiland***
National Energy Technology Laboratory
Pittsburgh, PA
Nathan.Weiland@netl.doe.gov

## ABSTRACT

Direct-fired supercritical $CO_2$ ($sCO_2$) power cycles are being explored as an attractive alternative to natural gas combined cycle (NGCC) plants with carbon capture and storage (CCS). Therefore, understanding their performance and cost potential is important for the commercialization of the technology. This study presents the techno-economic optimization results of natural gas-fired, utility-scale power plants based on the direct $sCO_2$ power cycle, which are lacking in public literature. To identify the optimum plant configuration, the study considered multiple cases with varying levels of thermal integration with the plant air separation unit (ASU). Several design variables for each power cycle configuration were identified and optimized to minimize the levelized cost of electricity (LCOE) for each case. The optimization design variables include the $sCO_2$ cooler outlet temperatures, recuperator approach temperatures, and pressure drops. High fidelity models for recuperators, coolers, and turbines were developed and used to capture the impact of design variables on plant efficiency and capital costs. The optimization was conducted using a combination of manual sensitivity analyses and automated derivative-free optimization algorithms available under NETL's Framework for Optimization and Quantification of Uncertainty and Sensitivity platform.

The optimized direct $sCO_2$ power plants offered similar or slightly higher plant efficiencies than the reference NGCC plants based on the F-class gas turbine with carbon capture and storage (CCS). The LCOE of the optimized direct $sCO_2$ plants is 13 to 17% higher than the reference NGCC plants with CCS due to high capital costs associated with the ASU and $sCO_2$ power block, though there is significant room for improvement due to the high uncertainty in component capital costs for these new plants. Recuperators make up over 50% of the $sCO_2$ power block costs. Consequently, any research and development efforts to reduce the recuperator capital costs will benefit the technology's commercialization. The study also presents preliminary results showing the impact of co-firing landfill gas and natural gas on plant efficiency, LCOE, and $CO_2$ emissions.

## INTRODUCTION

Direct-fired $sCO_2$ power cycles are an attractive alternative to NGCC plants (with CCS) due to their high efficiency and inherent ability to capture $CO_2$ at high rates. A simplified schematic of the direct-fired $sCO_2$ power cycle is shown in Figure 1. In these cycles, gaseous fuel is burned with oxygen in a highly dilute $sCO_2$ environment, with the combustion products driving a turbine to generate power. The thermal energy in the turbine exhaust is recuperated to heat the $CO_2$ diluent flow to the combustor. After recuperation, water is condensed out of the product stream, and a portion of the stream (primarily $CO_2$) is drawn from the cycle for further purification, compression, and storage. The rest of the stream is compressed to a pressure near the critical pressure, followed by additional cooling, and pumping to the cycle maximum pressure before pre-heating in the recuperator.

Allam and colleagues extensively studied the direct $sCO_2$ power cycles. [1, 2, 3] Commercialization of this technology is being pursued by NET Power, 8 Rivers Capital, and their collaborators, who built a 25 MWe demonstration plant in Laporte, Texas. In the natural gas-fired version of this cycle, their literature

* corresponding author(s)

DOI: 10.17185/duepublico/77275

suggests that net power plant efficiencies > 53% (HHV basis) are achievable with near 100% carbon capture. [3] Under slightly different assumptions, Foster Wheeler/IEAGHG modeling of this system yielded a net plant efficiency of 49.9% with 90% carbon capture. [4] Scaccabarozzi et al. performed sensitivity analyses and cycle optimization of the system modeled by IEAGHG and reported an HHV efficiency of 49.5 –50.0%. [5, 6] SwRI evaluated alternative natural gas-fired direct $sCO_2$ cycles with reported plant HHV thermal efficiencies ranging 46.5–51.1 percent. [7]

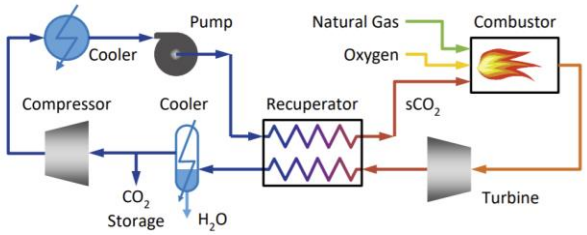


**Figure 1:** Schematic of a natural gas-fueled direct-fired $sCO_2$ power cycle

Prior NETL study presented a techno-economic analysis (TEA) of natural gas-fired version of the direct-fired $sCO_2$ power cycle. [8] Plant efficiency (HHV basis) was reported at 48.2%, which is higher than, or similar to, the reference NGCC plants with CCS (using F-frame and H-frame gas turbines). The COE of this plant is estimated at $79.2/MWh, compared to $83.3/MWh for the reference NGCC plant with CCS (using F-frame gas turbine). [8] These studies made several assumptions for modeling of the recuperators, turbine, and turbine blade cooling based on the best data available at the time. The primary objective of this paper is to build on the prior NETL natural gas-fired direct $sCO_2$ power cycle analyses to improve the accuracy of performance and economic modeling for components such as ASU, recuperators, coolers, and turbine. In particular, this study uses a high-fidelity cooled $sCO_2$ turbine model to estimate the turbine output and required turbine coolant flow. High-fidelity recuperator and cooler models are used to study the impact of design parameters such as temperature approach and pressure drop on both the plant efficiency and COE. The study also presents a pre-screening level analysis showing the impact of landfill gas (LFG) and natural gas co-firing on direct $sCO_2$ power plant efficiency, COE, and emissions.

## $SCO_2$ POWER PLANTS DESCRIPTION

A block flow diagram of the natural gas-fired direct $sCO_2$ plant modeled in this study is shown in Figure 2. Compressed natural gas (stream 14), pre-heated oxidant (stream 12), and pre-heated recycle diluent (stream 32) are fed to the $sCO_2$ oxy-combustor where combustion of the natural gas increases the temperature of mixture to the TIT. The effluent from the combustor (stream 34) is expanded in $sCO_2$ turbine. It is also important to emphasize that the combustion system for direct-fired $sCO_2$ plants is vastly different compared from that of traditional NGCC plants. Traditional NGCC plant combustors are air-fired and operate at pressures ~3.5 MPa [9] whereas direct-fired $sCO_2$ plant combustors are oxy-fired and operate at an order of magnitude higher pressures (~30 MPa) than traditional NGCC plant combustors. These differences will lead to vastly different combustion kinetics and combustor designs which can have a major impact on plant performance as well as capital costs.

The turbine exhaust (stream 35) pre-heats the incoming oxidant (stream 8) and recycle diluent (stream 20) streams in the recuperation train. Exiting the recuperation train, the cooled turbine exhaust (stream 39) is passed through the water knockout (KO) cooler to condense out water (stream 41) from the mixture. A portion of the recycle stream is purged from the cycle (stream 42) for further purification and compression in the CPU, to meet $CO_2$ pipeline standards for $O_2$, CO, $H_2O$, and other contaminants. The rest of the recycle stream is sent to the compression train. The recycle and purge stream flows are controlled to attain a TIT of 1204°C. In the compression train, a pre-compressor increases the pressure of recycle stream (stream 15) to ~100 bar and the compressed stream (stream 16) is cooled in the main cooler. A portion of the recycle stream (stream 18) is mixed with $O_2$ (stream 6) from the ASU to generate the oxidant stream (stream 7). The maximum mole fraction of $O_2$ in the oxidant stream is set to 23.5% based on guidance from ASU vendors. The oxidant stream (stream 7) and rest of the recycle stream (stream 19) are compressed to cycle maximum pressure in the oxidant compressor and boost pump respectively. Oxygen for the plant comes from a cryogenic ASU. An $O_2$ purity of 99.5% is chosen to minimize $N_2$ and Ar impurities, which increase the required compression power in the $sCO_2$ cycle, thereby reducing cycle efficiency. [9] This is partially offset by the increase in ASU power requirement needed to produce high-purity $O_2$ and also increases the cost of the ASU. The recuperation train is split into four stages to better manage thermal pinch points, provide the necessary turbine coolant flows, reduce high temperature material use, and for thermal integration with the ASU.

The LTR is designed to achieve condensation of water vapor from the hot, LP turbine exhaust stream (stream 36). To avoid an internal pinch point in the LTR, the hot side inlet (stream 38) temperature is typically at or close to its dew point so that water begins to condense at the ITR outlet. Integration of the process heat from the ASU occurs in parallel to the LTR and the ITR, where the specific heat capacity difference between hot and cold sides is highest. Ideally, the thermal integration should occur in the temperature range of LTR, ITR, and HTR2 to maximize heat recovery; however, due to lack of high temperature heat sources from the ASU, the thermal integration is limited to the LTR and ITR. The temperature of the diluent (stream 25) and oxidant (stream 10) streams exiting the ITR is set to 213.3°C. A portion of the diluent stream exiting the ITR is drawn (stream 24) to provide the necessary turbine blade coolant flow. The temperature of the diluent (stream 28) and oxidant (stream 11) streams exiting the HTR2 is set to 327.8°C. The rest of the turbine blade coolant (stream 29) is withdrawn from the diluent stream exiting the HTR2. An upper limit of 760°C was chosen for the turbine exhaust (stream 35) based on high temperature and pressure limits of nickel-based alloys, which represent a


DOI: 10.17185/duepublico/77275

major constraint on the system design. [8] Three different cases with varying levels of thermal integration with the ASU were considered in this study to systematically understand the impact of ASU thermal integration on plant efficiency and LCOE. The case description and matrix are presented in Table 1. Modeling assumptions for ASU compressors and intercoolers are based on a discussion with ASU vendors. For Case A, no thermal integration with the ASU was considered and the ASU main air compressor (MAC) and boost air compressor (BAC) were intercooled with water. For Case B, the intercooled MAC was replaced with an adiabatic compressor (no intercooling) for thermal integration with relatively hot air exiting the MAC. Heat is recovered from air exiting the MAC followed by an aftercooler to cool the air to the desired temperature. For Case C, thermal integration with both the ASU MAC and BAC was considered. The MAC is an adiabatic compressor (no intercooling, similar to Case B) and the BAC is a multi-stage intercooled compressor with the intercooler (IC) temperature set to have 5.6°C approach to the diluent stream temperature exiting the compression train (stream 20) to allow for thermal integration with ASU BAC ICs.

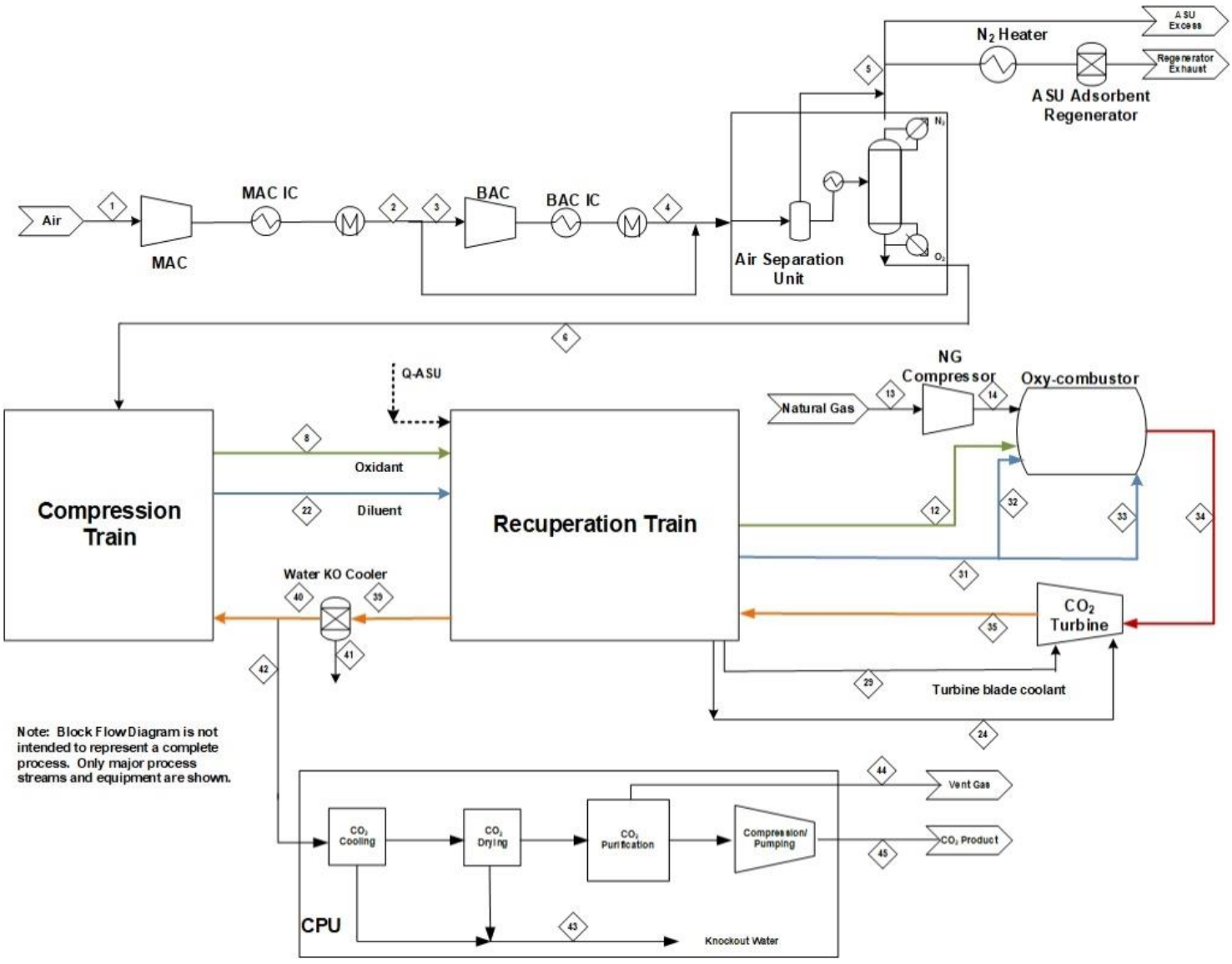



DOI: 10.17185/duepublico/77275

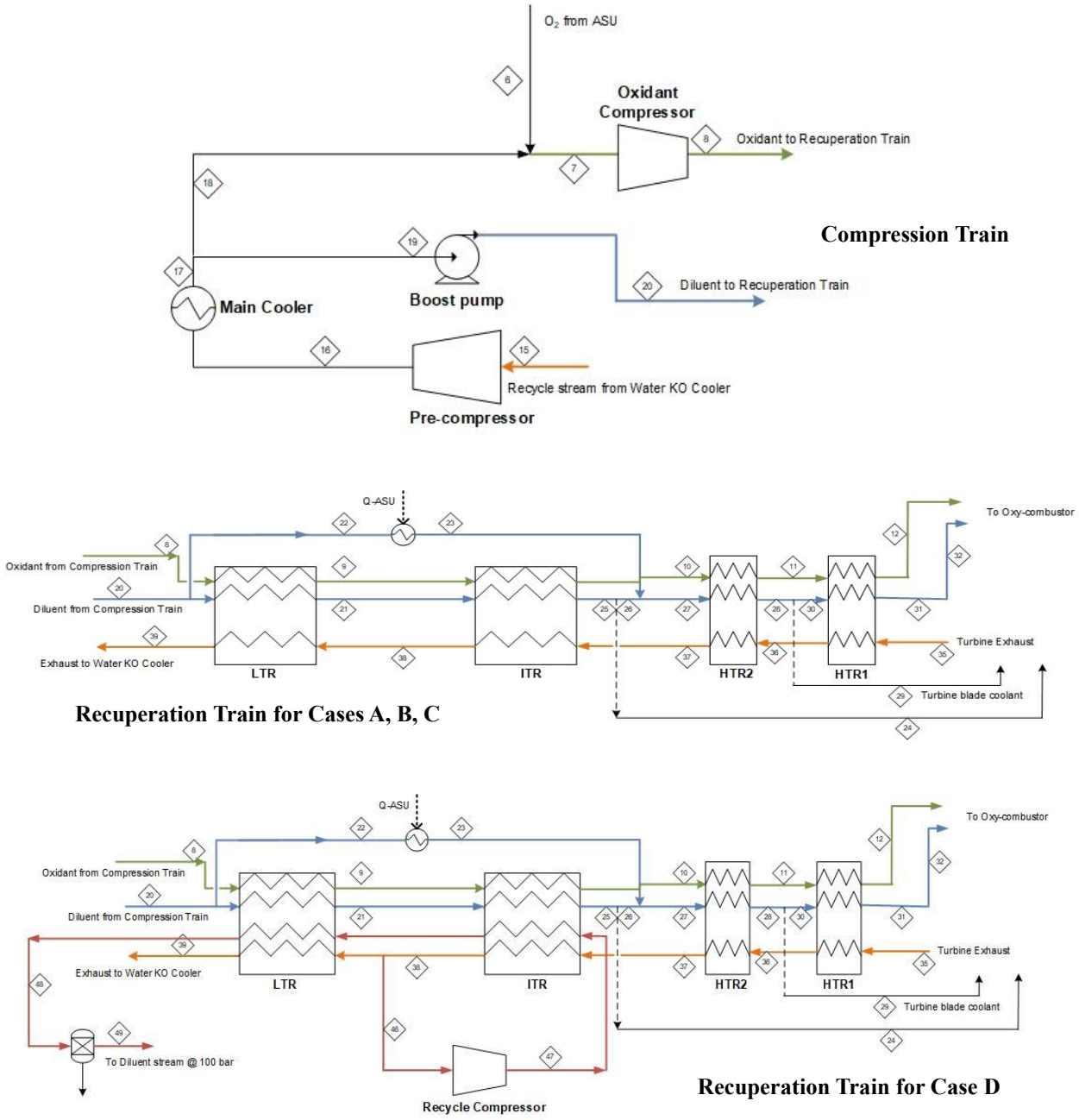


**Figure 2:** Block flow diagrams for natural gas-fueled direct-fired $sCO_2$ power plants considered in this study

In addition to the three cases presented in Table 1, an alternative case based on a patent from 8 Rivers was considered to increase the amount of heat recovered to the recuperation train. [10] This case is represented as Case D in the paper. A diagram of the recuperation train for Case D is shown at the bottom of Figure 2. A portion of the turbine exhaust exiting the ITR (stream 36) is bypassed and compressed in a recycle compressor to 100 bar (1,460 psi) that matches with the $O_2$ delivery pressure from the ASU. The hot $CO_2$ stream exiting the recycle compressor (stream 47) is sent back to the recuperation train to provide additional heat for the ITR and LTR. After exiting the LTR, the compressed $CO_2$ stream (stream 48) is cooled in a separate water knockout cooler and the resulting dried stream (stream 49) is mixed with the compressed $CO_2$ stream exiting the pre-compressor (stream 16). In addition to the heat supplied by the compressed recycle stream (stream 47), the recuperation train for Case D is also thermally integrated with the ASU MAC and BAC (similar to Case C). Based on the case descriptions, it can be noted that the


DOI: 10.17185/duepublico/77275

amount of additional heat supplied to the recuperation train increases from Case A to Case D, which improves the cycle efficiency but at the expense of increased auxiliary loads for the ASU and the recycle compressor (only for Case D).

| Case Description | ASU MAC Heat Recovery | MAC Intercooler Temperature | ASU BAC Heat Recovery | BAC Intercooler Temperature |
|---|---|---|---|---|
| Case A | No (Isothermal MAC) | 21.1°C | No (Isothermal BAC) | 21.1°C |
| Case B | Yes (Adiabatic MAC) | No intercooling | No (Isothermal BAC) | 21.1°C |
| Case C | Yes (Adiabatic MAC) | No intercooling | Yes (Isothermal BAC) | 5.6°C approach to diluent temperature entering LTR |

**Table 1:** Direct $sCO_2$ plants configuration matrix

## MODELING APPROACH

The design bases from NETL's Fossil Energy Baseline study [11] and Quality Guidelines for Energy System Studies (QGESS) series were adopted so that the results from this study would be consistent with the established results for reference NGCC plants. All the plants are assumed to be located at a generic plant site in the midwestern United States at sea level with an ambient dry bulb temperature of 15°C and 60% relative humidity. All the plants are assumed to have an 85% capacity factor with net power output of 650 MWe. Natural gas properties used in this study are taken from 2019 revision of the NETL QGESS document "Specification for Selected Feedstocks". [12]

### Performance Modeling Methodology

The thermodynamic performances of all the plants described in this study are based on the output from a steady-state model developed using Aspen Plus® software. In addition to the overall plant model, sub-system models for the cooled $sCO_2$ turbine, recuperators, $CO_2$ coolers/ICs were used for estimating their performance and cost. These sub-system models will be described briefly in the subsequent sections. For direct-fired $sCO_2$ power cycles, the working fluid is not pure $CO_2$ and changes composition at various points in the cycle. Due to limitations of the REFPROP property method for $sCO_2$ mixtures, the LK-PLOCK property method (based on the Lee-Kesler-Plöcker EOS) was used for modeling the direct $sCO_2$ power cycle. [13] For ASU and CPU components, the PENG-ROB physical property method was used.

For Case A, the ASU MAC was modeled as a three-stage compressor with two intercooling stages. The discharge pressure of the MAC was assumed to be 0.586 MPa with an isentropic efficiency of 87% for each stage. For the rest of the cases, the multi-stage water intercooled model was replaced with an adiabatic compression train with aftercoolers. As described earlier, the aftercooler uses recycle $CO_2$ exiting the compression train as the cold sink. The ASU BAC was modeled as a six-stage compressor with five intercooling stages. The discharge pressure of the BAC was assumed to be 11.38 MPa with an isentropic efficiency of 87% for each stage. The cold sink for Cases A and B is process water cooling whereas for Cases C and D, recycle $CO_2$ exiting the compression train is the cold sink.

Table 2 summarizes the $sCO_2$ power cycle design conditions used for all the cases in this study. [4, 5, 8] The oxy-combustor was modeled in Aspen Plus with a series of combustion reactions for the oxidizable components of the fuel and assuming 100 percent conversion of these fuel components. The amount of excess $O_2$ is based on the stoichiometric amount needed for complete combustion of the fuel stream entering the process, without regard to any oxidizable components in the recycle $sCO_2$ stream. The turbine inlet temperature (TIT) selected in Table 2 (1,204°C) is slightly lower than that of reference F-class gas turbine (TIT ≈ 1,371°C) selected in this study. Follow-on studies should consider TIT as a design variable for optimization.

| Section | Parameter | Value |
|---|---|---|
| **Combustor** | $O_2$ purity | 99.5% |
| | Excess $O_2$ | 0.1% |
| | Stages | 1 |
| | Pressure drop | 300 kPa |
| | Heat loss | Zero |
| **Turbine** | Inlet temperature | 1,204°C |
| | Inlet pressure | 30.0 MPa |
| | Outlet pressure | 2.98 MPa |
| | Blade cooling | See below |
| **$CO_2$ Pre-Compressor** | Stages | 5 |
| | Intercooling stages | 4 |
| | Isentropic efficiency | 85% |
| **Oxidant/Recycle compressor** | Stages | 1 |
| | Intercooling stages | 0 |
| | Isentropic efficiency | 85% |
| **Boost Pump** | Stages | 2 |
| | Intercooling stages | 1 |
| | Isentropic efficiency | 85% |

**Table 2:** $sCO_2$ power cycle design parameters [4, 5, 8]

The cooled $sCO_2$ turbine includes four stages and was modeled in Aspen Custom Modeler (ACM) based on a high-fidelity turbomachinery design to estimate the necessary coolant flowrates, cooled turbine efficiencies, turbine exhaust temperature (as well as stage temperature distribution), and power output. A cooled turbine analysis, which was originally


DOI: 10.17185/duepublico/77275

developed and validated for air-breathing gas turbines, [14] was reviewed and modified for $sCO_2$ working fluid. An analytical thermal stress analysis was conducted to determine coolant temperatures and cooling configurations to ensure safe operation for the disks and blades (i.e., without causing excessive thermal stress loads). The design for this study only considered internal cooling since the viability of film cooling in an $sCO_2$ environment has not yet been verified. Figure 3 shows the $sCO_2$ turbine configuration and introduction of coolant streams. As mentioned earlier, two coolant streams at 213.3°C and 327.8°C are drawn from the recuperation train (diluent stream exiting ITR, HTR2) for turbine blade cooling. The lower temperature stream is used to cool the third stage and the higher temperature stream is used to cool the first two stages to reduce thermal stresses. The fourth stage of the turbine is not cooled. Purge cooling is used to provide cooling to the rims and seals of the turbine and supplemental cooling for the disks and blades. The fraction of the purge flow varies for each stage, but it is in the range of 0.2–0.5 percent of the diluent flowrate. The range of purge cooling flow is determined from the typical ranges used in conventional gas turbines. The coolant used to cool the stator is directed to the casing to cool the turbine outer casing to reduce tip clearance related losses of the rotors. The purge cooling between the stator and rotor blades is supplied from the casing, whereas the purge cooling for the stator is supplied from the disk cavity. The cooling analysis showed that a thermal barrier coating is needed to provide thermal protection. Further details about the cooled turbine design equations and calculations can be found in Uysal et al. [15, 16]

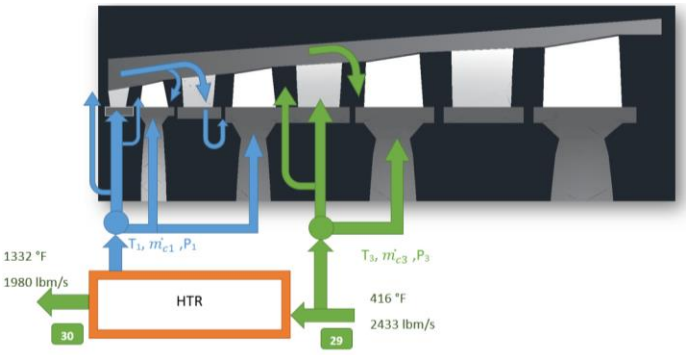


**Figure 3:** Single flow $sCO_2$ turbine configuration

The $sCO_2$ recuperators are envisioned to be compact diffusion-bonded heat exchangers, commercially known as printed circuit heat exchangers (PCHEs). A one-dimensional PCHE model was developed in the ACM platform for the design of the cycle recuperators. The cross-section of PCHE etched channels is mostly semi-circular with a channel width/diameter ($D_c$) varying from 1 – 5 mm. In this study, $D_c$ was varied for each of the recuperators to reduce the capital cost of the recuperation train. A high-angle channel design was adopted for the cold side and a low-angle channel design was adopted for the hot side using thermal-hydraulic correlations developed based on experimental data available in open literature. [17] The low-angle channel design for the hot side results in significantly lower pressure drops, which is advantageous despite having lower heat transfer coefficients compared to the high-angle channel design. The ratio between the number of hot and cold plates ($R_p$) was set to 2 for a more uniform distribution of pressure drop on hot and cold sides. To capture the sharp variation in thermo-physical properties near the critical point, the number of nodes along the z direction was set to 50. Further details of the PCHE model and validation can be found in Jiang et al. [18]

The $sCO_2$ cycle coolers and ICs are made up of adiabatic cooler bays. Adiabatic coolers are used in the $CO_2$ refrigeration industry to enhance the performance of $CO_2$ coolers during hot conditions. An Excel-based performance model of an adiabatic cooler bay was developed. The heat exchanger tube bundles are discretized into multiple sub-sections (N=10) to account for the non-linear variation in thermo-physical properties of $CO_2$. The model was validated to the data provided by the vendor. The adjustable inputs include $CO_2$ operating conditions, ambient air dry and wet bulb temperatures, and the number of discretization points (N) along the tube bundle length. The model iteratively calculates the number of required bays, total auxiliary fan power consumption and total water consumption rate to meet the desired operating conditions. Further modeling details, $CO_2$-side and air-side heat transfer and pressure drop correlations, can be found in Pidaparti et al. [19]

**Economic Analysis Methodology**

Plant capital costs in this study are estimated according to NETL's QGESS document [20]. The capital costs are defined at two levels: bare erected cost (BEC) and total plant cost (TPC), which are overnight costs expressed in 2018 base-year dollars. No process contingency costs are applied to $sCO_2$ specific components during optimization, which are more reflective of Nth-of-a-kind (NOAK) cost estimates.

All the $sCO_2$ power cycle components costs follow a general power law form:

$$C = aSP^b \times f_T$$

where $SP$ is the scaling parameter, $a$ and $b$ are the scaling coefficients, and $f_T$ is a temperature correction factor of the following form:

$$f_T = \begin{cases} 1 & if\ T_{max} < T_{bp} \\ 1 + c(T_{max} - T_{bp}) + d(T_{max} - T_{bp})^2 \end{cases}$$

where $T_{bp}$ is the temperature breakpoint which is 550°C, and $T_{max}$ is the maximum temperature rating of the component. The scaling parameters and coefficients are listed in Table 3. Except for recuperators and coolers, these values are taken from Weiland et al. [21]. Recuperators cost correlation use recuperator mass ($M_{recup}$) as the scaling parameter derived from vendor quotes. $M_{recup}$ is calculated using the PCHE model described earlier and captures the impact of design variables such as temperature approach, pressure drops etc. The recuperator cost correlation shown in Table 3 is only valid for PCHEs constructed


DOI: 10.17185/duepublico/77275

out of stainless steel 316. However, HTR1 experiences temperatures >700°C due to exposure to turbine exhaust. In order to withstand such high temperatures, HTR1 is broken into two separate sections (HTR1-LT and HTR1-HT). HTR1-LT is constructed out of stainless steel 316 (SS316) and HTR1-HT is constructed out of Inconel 740H (IN740H) to withstand temperatures as high as 760°C. The IN740H PCHE cost is calculated using the following cost algorithm, which includes a correction factor ($CF$) to account for difference in material costs for SS316 (material cost = $6.8/lb) and IN740H (material cost = $30.0/lb):

$$C = 1{,}371\ M^{0.7842} * (CF)$$

$$CF = \left(\frac{30}{6.8}\right)$$

It should be noted the IN740H PCHE cost correlation is not compared/validated against any vendor quote and also does not consider the difference in fabrication costs between IN740H and SS316 PCHEs. Therefore, it carries a high degree of uncertainty compared to the SS316 PCHE cost correlation. To reduce the total capital cost of HTR1, a sensitivity analysis was conducted to determine an appropriate breakpoint temperature between HTR1-LT and HTR1-HT sections. As shown in Figure 4, HTR1 capital cost exhibits a minimum around temperature breakpoint of ~600°C.

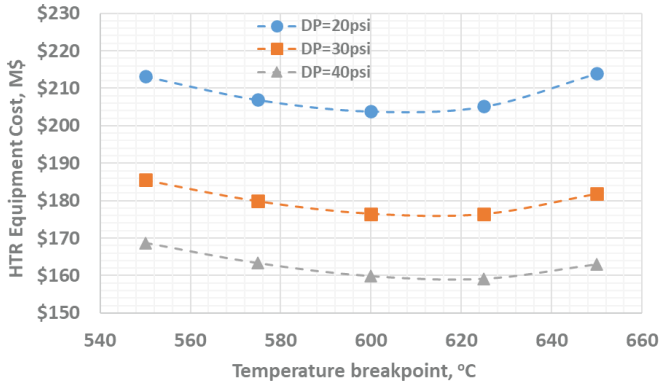


**Figure 4:** HTR1 capital cost as a function of breakpoint temperature for various pressure drops

| Component | Scaling parameter (Units) | Coefficients | | | |
|---|---|---|---|---|---|
| | | ***a*** | ***b*** | ***c*** | ***d*** |
| Recuperators (HTR2, ITR, LTR) | $M_{Recup}$ (kg) | 1,371 | 0.78 | 0 | 0 |
| $sCO_2$ compressors | $\dot{V}_{in}$ ($m^3/s$) | 6,220,000 | 0.11 | 0 | 0 |
| Generator | $\dot{W}_e$ ($MW_e$) | 108,900 | 0.55 | 0 | 0 |
| Compressor motor | $\dot{W}_e$ ($MW_e$) | 399,400 | 0.61 | 0 | 0 |
| Adiabatic coolers | $N_{bays}$ | 124,933 | 1.00 | 0 | 0 |
| Water Knockout cooler | $UA$ (W/K) | 49.45 | 0.76 | 0 | 0 |

**Table 3:** Cost scaling parameters and coefficients for the $sCO_2$ power cycle components

The equipment cost of coolers and intercoolers are scaled linearly with the number of adiabatic cooler bays ($N_{bays}$) calculated by the cooler model. The coefficient $a$ for the coolers represents the cost per bay quoted by the vendor. The most novel component of the cycle is the combustor and turbine, for which no cost estimates exist in the public domain at any scale. The approach taken with this component is to combine the cost of a similarly-sized gas turbine (without the compressor) with the cost of a high-pressure outer casing similar to those used for HP steam turbines. Costs for these components are well-known and combine to constitute a cost estimate for a mature, NOAK direct $sCO_2$ turbine and combustor, albeit with a high degree of uncertainty. Any cost adjustments based on turbine output were calculated using the scaling exponent from NETL's QGESS. [22]

ASU capital cost was derived from an existing vendor quote for IGCC applications. The capital cost was scaled based on the $O_2$ flowrate using the scaling parameter from NETL's QGESS [22] and the costs are adjusted to 2018 dollars using the Chemical Engineering Plant Cost Index. It should be noted that the cryogenic ASU requirements for direct $sCO_2$ plants is different from the requirements for IGCC applications. IGCC applications require higher $N_2$ product pressure, which require use of higher-pressure columns in the ASU. Therefore, there might be significant uncertainty associated with use of this vendor quote for direct $sCO_2$ plant applications.

Operation and maintenance (O&M) costs are divided into two categories: fixed O&M costs that are independent of plant operation hours (e.g., labor, overhead, etc.), and variable O&M costs that are proportional to the power generation (e.g., consumables, waste disposal, maintenance materials). The variable O&M and fuel costs are multiplied by an assumed capacity factor of 85% to arrive at the actual annual expenditure. The captured $CO_2$ transportation and storage (T&S) costs are estimated as $10/tonne [23]. The assumed levelized natural gas price is $4.19/GJ ($4.42/MMBtu), on an HHV basis, delivered to the Midwest, and reported in 2018 U.S. dollars. Fuel costs are levelized over an assumed 30-year plant operational period with an assumed on-line year of 2023.

The levelized cost of electricity (LCOE) is reported on a $/MWh basis and consists of contributions from the O&M costs (fixed, variable, and fuel)

, $CO_2$ T&S costs, and the annualized capital over the assumed 30-year lifetime of the plant. Additional details on the cost estimating methodology and other economic assumptions can be found in Gerdes et al. [20]. All the economic assumptions are consistent with the reference NGCC plants to ensure a fair comparison between both the technologies.

## OPTIMIZATION APPROACH

The overall plant optimization was conducted in two steps. In the first step, design parameters related to the recuperation train were optimized. This includes conducting a manual sensitivity analysis with respect to LTR cold end approach temperature, oxidant $O_2$ mole fraction, and recuperation train total pressure drops. To optimize the recuperation train total pressure drop, a manual sensitivity analysis was conducted assuming the same


DOI: 10.17185/duepublico/77275

pressure loss ($P_{Loss}$) for each recuperator as the starting point; the distribution of $P_{Loss}$ across the recuperation train was optimized using automated optimization solvers in the FOQUS platform [24] to minimize the recuperation train capital cost. For automated optimization, the covariance matrix adaption evolution strategy (CMA-ES) solver, which belongs to the class of evolutionary algorithms, was selected. [25] Recuperator channel diameters were also optimized using the CMA-ES optimization solver to minimize the recuperation train capital costs. Once the recuperation train design parameters were optimized, the compression train-related design parameters were optimized in the second step. The compression train optimization included conducting manual sensitivity analyses with respect to cooler/IC temperatures, and cooler/IC pressure drops. For each cooler temperature, the compression pressure profiles were optimized using the CMA-ES optimization solver to minimize the compression train power consumption. Once the compression train optimization was complete, the optimum recuperation train design parameters were verified by conducting a perturbation analysis as the final step of optimization.

**Sample Optimization Results**

Figure 5 presents sample optimization results showing the impact of LTR cold end approach temperature ($T_{App,LTR}$) and recuperator pressure loss ($P_{Loss}$) on the plant efficiency and LCOE. These sample results are generated for Case C (thermal integration with ASU MAC and BAC), but similar trends were noticed for all the cases. For these sample results, $P_{Loss}$ (defined below) is assumed to be same for all the recuperators (LTR, ITR, HTR2, HTR1-LT, HTR1-HT).

$$P_{Loss} = \frac{\Delta P_{cold} + \Delta P_{hot}}{P_{hot,in} + P_{cold,in}}$$

From Figure 5, increasing $T_{App,LTR}$ or $P_{Loss}$ reduces the plant efficiency but the plant LCOE presents an optimum value with respect to both $T_{App,LTR}$ and $P_{Loss}$. Increasing $T_{App,LTR}$ reduces the recuperation trian effectiveness and results in lower combustor inlet temperature. This leads to higher natural gas and $O_2$ flow requirements to achieve the desired TIT of 1204°C, thereby reducing the plant efficiency. Likewise, increasing $P_{Loss}$ directly contributes to lower plant efficiency by increasing the compression train power consumption to make up for the pressure losses in the recuperation train. However, increasing $T_{App,LTR}$ and $P_{Loss}$ also leads to lower recuperation train capital costs due to higher driving forces and lower heat transfer area requirements. These competing factors lead to optimum LCOE values with respect to both $T_{App,LTR}$ and $P_{Loss}$. From these sample results, it is clear that Case C considered in this study can achieve plant efficiencies as high as 50 percent (HHV basis) reported in the literature. However, the resulting capital costs and LCOE would be high in order to achieve these higher plant efficiencies.

The next step of the recuperation train design optimization is to conduct an automated optimization of the recuperation train to identify appropriate PCHE channel diameters and $P_{Loss}$ for individual recuperators to minimize the total recuperation train capital costs. Table 4 shows the $P_{Loss}$ for individual recuperators before and after optimization using the CMA-ES solver in the FOQUS platform. Before the optimization, $P_{Loss}$ for all the recuperators was assumed to be 0.2975%. After the optimization, a significantly higher $P_{Loss}$ is calculated for the Inconel 740H PCHE (HTR1-HT); $P_{Loss}$ is lowest for LTR, which has the lowest design temperature. As a result of the optimization, recuperation train equipment cost decreased from 345.5 M$ to 238.0 M$ and the LCOE decreased from $84.4/MWh to $80.5/MWh. These results highlight the importance of recuperation train optimization to reduce the direct $sCO_2$ plant LCOE, albeit at the expense of reduced plant efficiency.

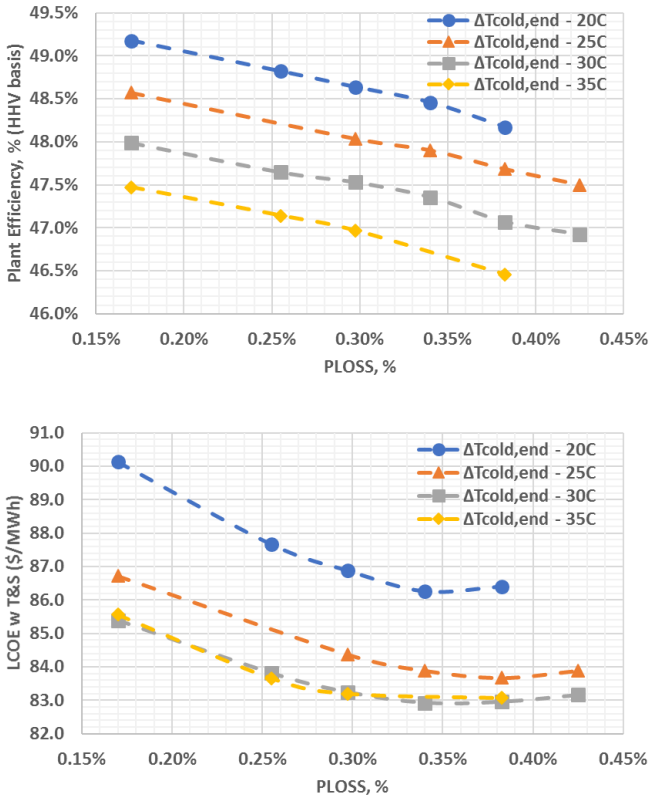


**Figure 5:** Impact of LTR cold end approach temperature and recuperator pressure loss on plant efficiency and LCOE

| Design Variables | Pre-Optimization | Post-Optimization |
|---|---|---|
| $P_{Loss,LTR}$ | 0.2975% | 0.188% |
| $P_{Loss,ITR}$ | 0.2975% | 0.226% |
| $P_{Loss,HTR2}$ | 0.2975% | 0.226% |
| $P_{Loss,HTR1-LT}$ | 0.2975% | 0.329% |
| $P_{Loss,HTR1-HT}$ | 0.2975% | 0.973% |
| Recuperation train equipment cost, M$ | 345.5 | 238.0 |
| LCOE with T&S ($/MWh) | 84.4 | 80.5 |

**Table 4:** Optimization of $P_{Loss}$ distribution using CMA-ES optimization solver


DOI: 10.17185/duepublico/77275

Figure 6 presents the impact of $sCO_2$ cooler/IC temperature ($T_{cooler}$) on the plant efficiency and LCOE. For each cooler temperature, the compression train pressure profiles as well as cooler/IC pressure drops are optimized to minimize the plant LCOE. Optimum compression pressure profiles for each cooler temperature are presented in Table 5. The pre-compressor outlet pressure is set to 10 MPa for all the cases to provide necessary mixing with $O_2$ from the ASU to generate the oxidant stream. The pre-compressor stage outlet pressures decrease with the cooler temperature. The pre-compressor stage 4 outlet pressure is close to the saturation/pseudo-critical pressure of the mixture. From Figure 6, decreasing $T_{cooler}$ from 26°C to 20°C improves the plant efficiency by 1.4 percentage points and reduces the LCOE by ~3.8%. Any further reduction in $T_{cooler}$ below 20°C improves the plant efficiency but increases the LCOE due to higher capital costs associated with coolers/ICs. It should be noted that these results are only valid for fixed ambient design conditions used in this study.

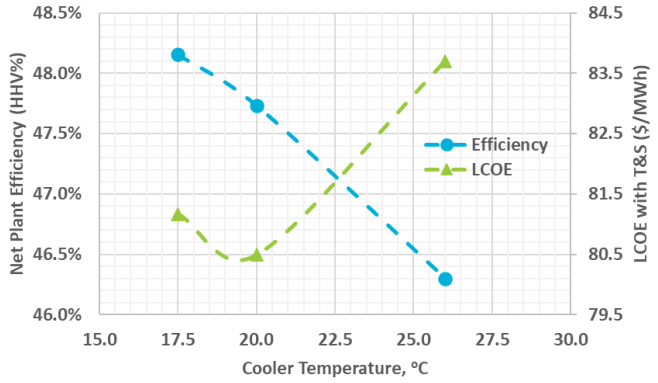


**Figure 6:** Impact of cooler/IC temperature on plant efficiency and LCOE

| $T_{cooler}$ | 17.5°C | 20.0°C | 26.0°C |
|---|---|---|---|
| Pre-compressor stage1 outlet | 3.58 | 3.67 | 3.66 |
| Pre-compressor stage2 outlet | 4.67 | 4.92 | 4.87 |
| Pre-compressor stage3 outlet | 5.84 | 6.19 | 6.23 |
| Pre-compressor stage4 outlet | 6.50 | 6.82 | 7.45 |
| Boost pump stage1 outlet | 17.51 | 17.74 | 17.51 |

**Table 5:** Optimization pressure profiles (in MPa) for different cooler/IC temperatures

## OPTIMIZED DIRECT $SCO_2$ PLANTS

Table 6 presents optimized design variables for all the cases (Case A through Case D) considered in this study. Optimized compression train design parameters are similar for all the cases, but the optimized recuperation train design parameters are impacted by the amount of thermal integration with the ASU. Optimum $T_{App,LTR}$ increases with the amount of thermal integration with the ASU due to tighter approach temperatures within the recuperation train. For example, optimum $T_{App,LTR}$ for Case A (no heat recovery from the ASU) is 1.5°C but that value increases to 25.0°C for Case C (heat recovery from both the ASU MAC and BAC) to reduce the recuperation train capital cost. Likewise, the optimum $P_{Loss}$ distribution is also impacted by the amount of thermal integration with the ASU. For example, optimum $P_{Loss}$ for Inconel 740H PCHE (HTR1-HT) increases from 0.872% to 0.973% going from Case A to Case C, again, to reduce the recuperation train capital cost.

| Design Variables | Case A | Case B | Case C | Case D |
|---|---|---|---|---|
| **Recuperation Train Design Parameters** | | | | |
| $T_{App,LTR}$, °C | 1.5 | 15.0 | 25.0 | 25.0 |
| $D_{c,LTR}$, mm | 1.1 | 1.0 | 1.2 | 1.1 |
| $D_{c,ITR}$, mm | 1.1 | 1.1 | 1.3 | 1.1 |
| $D_{c,HTR2}$, mm | 2.6 | 2.5 | 2.3 | 2.0 |
| $D_{c,HTR1-LT}$, mm | 1.7 | 1.7 | 1.6 | 1.4 |
| $D_{c,HTR1-HT}$, mm | 1.6 | 1.6 | 1.4 | 1.1 |
| $P_{Loss,LTR}$ | 0.276% | 0.224% | 0.188% | 0.183% |
| $P_{Loss,ITR}$ | 0.273% | 0.255% | 0.226% | 0.211% |
| $P_{Loss,HTR2}$ | 0.204% | 0.224% | 0.226% | 0.217% |
| $P_{Loss,HTR1-LT}$ | 0.307% | 0.316% | 0.329% | 0.312% |
| $P_{Loss,HTR1-HT}$ | 0.872% | 0.949% | 0.973% | 0.957% |
| Oxidant $O_2$ mole fraction | 13.3% | | | |
| **Compression Train Design Parameters** | | | | |
| $T_{cooler}$, °C | 20.0 | | | |
| $\Delta P_{PCIC1}$, kPa | 103.4 | | | |
| $\Delta P_{PCIC2}$, kPa | 103.4 | | | |
| $\Delta P_{PCIC3}$, kPa | 34.5 | | | |
| $\Delta P_{PCIC4}$, kPa | 13.8 | | | |
| $\Delta P_{MC}$, kPa | 103.4 | | | |
| $\Delta P_{PIC}$, kPa | 103.4 | | | |
| Pre-compressor stage1 outlet, MPa | 3.67 | | | |
| Pre-compressor stage2 outlet, MPa | 4.92 | | | |
| Pre-compressor stage3 outlet, MPa | 6.19 | | | |
| Pre-compressor stage4 outlet, MPa | 6.82 | | | |
| Boost pump stage1 outlet, MPa | 17.74 | | | |

**Table 6:** Optimized design variables for cases A through D

Table 7 (Refer to ANNEX A) provides a summary of the performance and detailed auxiliary power breakdown for the optimized direct $sCO_2$ plants along with reference NGCC plants. The reference B31B.90 and B31B.97 cases are state-of-the-art F-class NGCC plants with 90% and 97% $CO_2$ capture respectively. Details regarding performance modeling and economic analysis for the reference cases can be found in NETL's Fossil Energy Baseline report. [11] For comparison purposes, the natural gas flow rate for all the direct $sCO_2$ plants is set to the value used in the reference F-class NGCC plants. The following observations can be made when comparing the performance of the direct $sCO_2$ power plants with the reference NGCC plants:

- The optimized direct $sCO_2$ plants offered plant efficiencies in the range of 46.4 – 48.2%. These efficiencies are in line with the state-of-the-art F-class NGCC plants with $CO_2$ capture rates of 97%. However, direct $sCO_2$ plants can achieve capture rates as high as 99%.
- All the direct $sCO_2$ plants have a higher gross power output than the reference B31B.90, B31B.97 cases. However, the auxiliary power requirement for the direct $sCO_2$ plants is significantly higher than the reference NGCC plants primarily due to the ASU auxiliary load and natural gas compression. The ASU is not needed for the reference


DOI: 10.17185/duepublico/77275

NGCC plants due to the use of a post-combustion $CO_2$ capture system.

- The ASU power consumption increases as the heat recovery from the ASU increases. For example, ASU MAC and BAC power consumption increases from ~128 MWe to ~146 MWe going from Case A to Case C. However, this higher ASU power consumption is more than offset by the higher gross power output due to increased heat recovery.
- Thermal integration with the ASU is needed to achieve higher plant efficiencies. For example, optimized Case A has plant efficiency of 46.4% but that value increases to 47.7% for Case C despite having higher LTR cold approach temperatures (see Table 6). The likelihood of achieving >50% plant efficiency (HHV basis) is low for the direct $sCO_2$ plants without thermal integration with the ASU.
- Out of all the direct $sCO_2$ plants, Case D, which is based on the patent from 8 Rivers, offered the highest plant efficiency. This case also represents maximum heat integration with the ASU as well as heat integration with compressed recycle $CO_2$ gas.
- Water consumption of all the direct $sCO_2$ plants is significantly lower than the reference NGCC plants. Significant water reduction for the $sCO_2$ plants is primarily due to differences in cooling technologies (adiabatic versus wet cooling) as well as elimination of intrinsic water losses arising from the bottoming Rankine cycle such as from blowdown.

Table 8 (Refer to ANNEX A) shows the capital cost summary for all the optimized direct $sCO_2$ plants along with the reference NGCC plants. Figure 7 shows the LCOE breakdown for these cases. The following observations can be made when comparing the economics of the direct $sCO_2$ power plants with the reference NGCC plants:

- LCOE of the direct $sCO_2$ power plants are 13–23% higher than the reference NGCC plants. The higher LCOE is primarily due to higher capital costs associated with the cryogenic ASU and $sCO_2$ power block.
- TPCs of the direct $sCO_2$ power plants are 35–50% higher than the reference NGCC plants on a $/kWe basis. From Table 8, TPC of the cryogenic ASU for the direct $sCO_2$ plants is on par with the post-combustion $CO_2$ capture system TPC (Flue Gas Cleanup & Piping sub-account from Table 8) used in the reference NGCC plants. However, as noted earlier, there is uncertainty associated with the ASU vendor quote used for this study. BOP capital costs for the direct $sCO_2$ power plants are similar to that of the reference NGCC plants.
- $sCO_2$ power block capital costs are over twice that of the combined gas turbine, HRSG, and steam turbine capital costs in the NGCC plants. These differences arise from the need for additional heat exchangers (recuperators, multiple coolers, and ICs within the compression train) for direct $sCO_2$ power cycles. From Table 8, recuperators (HTR, ITR, and LTR) make up nearly 50% of the total $sCO_2$ power block costs. Coolers and ICs make up an additional 23 percent. Therefore, combined together, heat exchangers makeup 70–75% of the total $sCO_2$ power block costs.
- Thermal integration with the ASU not only improves the plant efficiency but also improves the plant economics and LCOE. For example, going from Case A to Case C, the plant TPC ($/kWe basis) and LCOE decreases by 1.3% and 2%, respectively. Thermal integration with the ASU increases the recuperation train capital costs as can be seen in Table 8. However, this increase in the power block capital costs is more than offset by higher power generation resulting from thermal integration with the ASU.
- Out of all the direct $sCO_2$ plants, Case C offered the lowest LCOE. Despite having higher plant efficiency, LCOE of the Case D is higher than the rest of the cases primarily due to additional capital expenses associated with the recycle compressor, additional water knockout cooler, etc. Therefore, heat integration with compressed recycle gas might not be an economical choice. However, if low-cost recuperators are developed in the future, the concept might present an attractive opportunity for additional heat beyond what can achieved with ASU thermal integration alone.

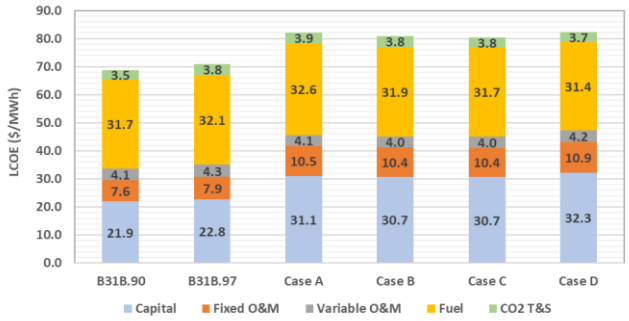


**Figure 7:** LCOE breakdown for all the optimized direct $sCO_2$ plants and reference NGCC plants

**Additional Sensitivities**

Figure 8 presents the impact of ASU capital cost reduction on the plant LCOE. As mentioned earlier, the ASU capital cost might carry a large degree of uncertainty due to the use of a vendor quote that is intended for IGCC applications. For example, the ASU capital cost used in the current study is ~$843/kWe but the ASU capital cost reported in the IEAGHG study is nearly 50 percent lower (~$440/kWe). [4] Consequently, a 50% reduction in the ASU capital cost leads to nearly 10% reduction in the plant LCOE making the technology much more competitive with the reference NGCC plants using a post-combustion capture system.


DOI: 10.17185/duepublico/77275

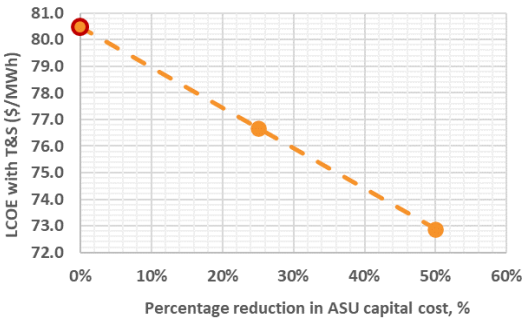


**Figure 8:** Impact of ASU capital cost reduction on LCOE

Another area of uncertainty in this study is associated with the Inconel 740H PCHE cost correlation. As described previously, the IN740H PCHE cost correlation includes a correction factor ($CF$) to account for the difference in material costs between IN740H and stainless steel 316. However, this approach is largely unvalidated and a sensitivity analysis was conducted to the $CF$ as presented in Figure 9. Decreasing the $CF$ from the base case of 4.4 to 3.0 reduces the LCOE by 2%. A lower correction factor can be a result of a more accurate cost algorithm accounting for differences in material as well as fabrication costs for IN740H PCHE. Alternatively, low-cost nickel alloys such as Inconel 625 can be used in place of IN740H to reduce the cost of the HTR.

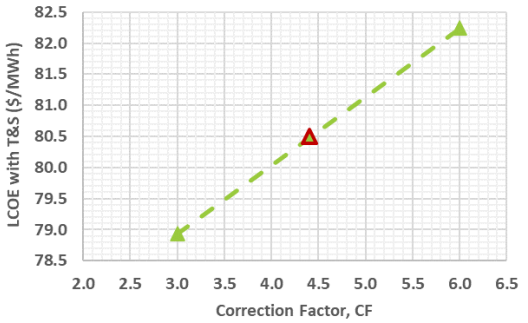


**Figure 9:** Impact of IN740H PCHE correction factor on LCOE

## IMPACT OF LANDFILL GAS CO-FIRING

This section presents the impact of LFG and natural gas co-firing on the direct $sCO_2$ plant efficiency, LCOE, and $CO_2$ emissions. LFG is a product of the decomposition of organic material (e.g., municipal solid waste) under anaerobic conditions. For a typical U.S. municipal solid waste, LFG contains 50–55% methane, 45–50% $CO_2$, and 2–5% other gases such as $N_2$ and sulfides, etc., along with less than 1% of non-methane organic compounds and trace amounts of inorganic compounds. For this study, the LFG composition was assumed to be 50% methane and 50% $CO_2$ (vol% basis) representing a generic site based on EPA recommendation. [26] Most landfills in the United States capture and flare the LFG to reduce methane emissions since methane is a significantly more potent greenhouse gas than $CO_2$. However, energy recovery systems can make use of this captured LFG to produce heat (boilers, kilns), generate electricity, or produce renewable natural gas.

For this study, the LFG gas collection and control system (GCCS) capital costs and annual O&M costs are estimated using EPA's LFGcost-Web Excel-based application. [27] LFG fuel price depends on the amount of treatment needed among other factors. For this study, the EPA-recommended value of $1.75/MMBtu was used as the LFG fuel price. [27] This is ~40% cheaper than the natural gas price assumed in the current study. LFG pre-purification steps (such as water and siloxanes removal) were assumed to be part of the assumed LFG fuel price.

Captured LFG is compressed from near atmospheric pressure to the combustor pressure of ~300 bar in a multi-stage intercooled compressor (total stages = 10). The maximum compression temperature is limited to 150°C to avoid LFG autoignition at high temperatures due to $O_2$ intrusion from air during compression. [28] Compression of LFG also presents an additional opportunity for thermal integration with the recuperation train and to improve plant efficiency. The LFG compressor intercooler temperature is set to have a 5.6°C approach to the recycle $CO_2$ stream exiting the power cycle compression train to allow for thermal integration. The stage isentropic efficiency is assumed to be 85%.

Figure 10 shows the impact of LFG and natural gas co-firing on the plant efficiency. Increasing the LFG co-firing from 0% to 50% decreases the plant efficiency by 0.3 percentage points. As the amount of LFG co-firing increases, the auxiliary loads associated with LFG compression, CPU increase. This is partially offset by higher cycle efficiency due to higher heat recovery from LFG compression. Consequently, the overall impact of LFG co-firing on plant efficiency is minimal.

Plant LCOE increases with LFG co-firing primarily due to the higher capital costs associated with the $sCO_2$ power block, LFG GCCS, and CPU. The power block capital cost increases with the LFG co-firing primarily due to higher capital costs associated with HTR. As the LFG co-firing increases, the amount of heat recovered from LFG compression increases leading to tighter approach temperatures within the recuperation train. The minimum temperature approach decreases from 6.9°C for 0% LFG co-firing to 3.1°C for 50% LFG co-firing. However, it should be pointed out that no attempt was made to optimize the recuperation train for different levels of LFG co-firing. Optimizing the LTR cold end approach temperature and the recuperators $P_{Loss}$ distribution can lead to lower LCOEs than the values presented in Figure 10. In addition to higher capital costs, O&M costs increase with LFG co-firing due to costs associated with the LFG GCCS. Increased LFG co-firing also leads to higher levels of $CO_2$ capture, which increases the $CO_2$ T&S costs. Overall, the increase in capital costs, O&M costs, and $CO_2$ T&S costs is partially offset by the lower fuel costs (due to lower LFG fuel price). As a result, increasing LFG co-firing from 0% to 50% increases the LCOE by 3% with only a marginal LCOE increase up to 30% LFG co-firing.


DOI: 10.17185/duepublico/77275

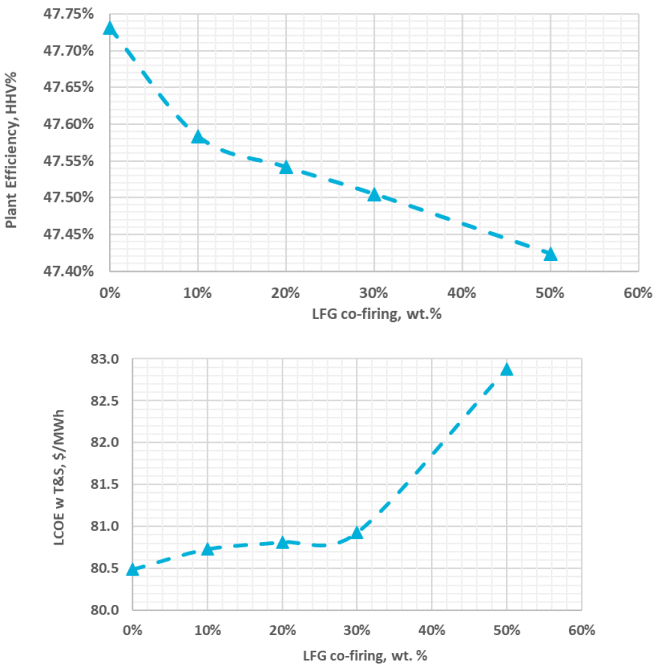


**Figure 10:** Impact of LFG co-firing on plant efficiency and LCOE

Figure 11 presents the impact of LFG co-firing on the net $CO_2$ emissions. The net $CO_2$ emissions for the plant are calculated using two methods from the literature. In Method1, the $CO_2$ emissions from LFG co-firing are offset from the plant $CO_2$ emissions. [28] Flaring of 1 kg of LFG generates 1.46 kg of $CO_2$ emissions assuming 100% combustion of the methane in LFG. Net $CO_2$ emissions are calculated by assuming that 50% of these flared $CO_2$ emissions are from biomass sources. [28] In Method2, the avoided $CO_2$ emissions from the use of LFG instead of natural gas are offset from the plant $CO_2$ emissions to calculate the net $CO_2$ emissions. Since LFG is considered as a renewable energy source, use of LFG can offset the need for natural gas fuel. The avoided $CO_2$ emissions from use of LFG instead of natural gas are calculated using EPA's LFGCost-Web Excel-based application. [27] Using both of the methods, the direct $sCO_2$ plants have the potential to achieve net-zero $CO_2$ emissions for 3–4% LFG co-firing. Due to high inherent $CO_2$ capture rates, direct $sCO_2$ plants have a strong potential for net negative $CO_2$ emissions when co-firing LFG and natural gas. For example, increasing the LFG co-firing rate to 50% results in net negative $CO_2$ emissions of 78–94 $kgCO_2/MWh$. It should be noted the net $CO_2$ emissions presented in Figure 11 did not consider the $CO_2$ emissions associated with the upstream chain aspects of LFG and natural gas supply. For example, $CO_2$ emissions associated with LFG leakage from the gas collection system or natural gas transportation are ignored in the calculations. As such, these results should be treated as a screening type analysis to utilize LFG for power generation at utility scale. Future studies should consider a life-cycle analysis in order to estimate the net $CO_2$ emissions more accurately. Conducting a life-cycle analysis will likely lead to higher required LFG co-firing rates in order to achieve net-zero $CO_2$ emissions.

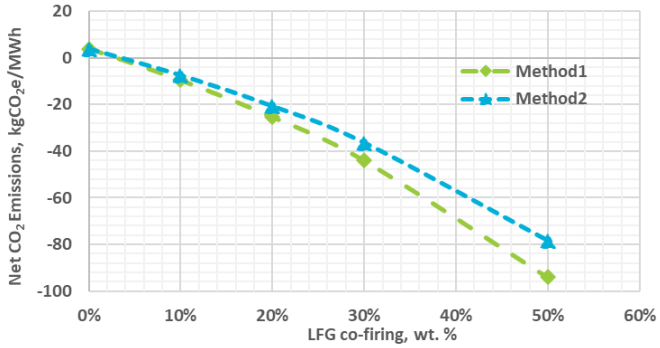


**Figure 11:** Impact of LFG co-firing on net $CO_2$ emissions

## SUMMARY AND CONCLUSIONS

This study presented the techno-economic optimization results for natural gas fueled direct $sCO_2$ plants. To improve the modeling accuracy, the plant Aspen Plus model included high-fidelity sub-system models for the air separation unit, cooled $sCO_2$ turbine, PCHE recuperators, and adiabatic coolers. Plant optimization was conducted using a combination of manual sensitivity analyses and automated optimization wherever possible to minimize the plant LCOE. Optimization variables included parameters related to the recuperation train (temperature approach, pressure drops, PCHE channel diameters) and the compression train (cooler temperature, compression pressure profiles, cooler/IC pressure drops). The study also considered various levels of thermal integration between the ASU and the recuperation train to investigate the impact on plant efficiency and LCOE. Results indicate that thermal integration of power cycle with both the ASU MAC and BAC is needed to achieve high plant efficiencies (>50% on HHV basis). However, achieving such high plant efficiencies would require tight recuperator approach temperatures and low $CO_2$ pressure drops, which increases the $sCO_2$ power block capital costs and the plant LCOE. Optimizing the design parameters while considering their impact on both plant efficiency and LCOE resulted in a plant efficiency (HHV basis) of 47.7% and LCOE (with $CO_2$ T&S) of $80.5/MWh. Compared to a state-of-the-art NGCC plant with CCS (using an F-class gas turbine and 97% $CO_2$ capture), the optimized direct $sCO_2$ plant has a 0.7 percentage point higher plant efficiency and 13.5% higher LCOE while offering a higher $CO_2$ capture rate of 98.5%. Uncertainty might exist in the ASU capital cost estimates and based on the sensitivity analysis conducted, a 50% reduction in the ASU capital cost would decrease the direct $sCO_2$ plant LCOE by 9.5%, which makes the technology competitive with the state-of-the-art NGCC plants with CCS. Additional economic improvements can be achieved by reducing the capital cost of PCHE recuperators operating at temperatures > 600°C, which would require the use of nickel alloys.


DOI: 10.17185/duepublico/77275

A screening type analysis was conducted to investigate the impact of co-firing LFG and natural gas on direct $sCO_2$ plant efficiency, LCOE, and emissions. Increasing the LFG co-firing rate from 0% to 50% (weight basis), decreased the plant efficiency by 0.3 percentage points and increased the LCOE by 3%. Due to high inherent $CO_2$ capture rates, direct $sCO_2$ plants have the potential to achieve net-negative $CO_2$ emissions from LFG and natural gas co-firing. Overall, this study presents the clearest picture of the cost and performance potential for direct $sCO_2$ power cycles in the public literature and identifies areas of research and development that could expedite the commercialization of this technology.

## NOMENCLATURE

| | |
|---|---|
| Ar | - Argon |
| ASU | - Air separation unit |
| BAC | - Boost air compressor |
| BFD | - Block flow diagram |
| BOP | - Balance of Plant |
| CCS | - Carbon capture and storage |
| CMA-ES | - Covariance matrix adaption evolution strategy |
| COE | - Cost of electricity |
| CPU | - $CO_2$ purification unit |
| CTM | - Cooled turbine model |
| DP | - Pressure drop |
| EPA | - Environmental protection agency |
| FOQUS | -Framework for Optimization and Quantification of Uncertainty and Sensitivity |
| GCCS | - Gas collection and control system |
| HHV | - Higher heating value |
| HRSG | - Heat recovery steam generator |
| HTR | - High temperature recuperator |
| IC | - Intercooler |
| IEAGHG | - International Energy Agency Greenhouse Gas Research Programme |
| IGCC | - Integrated gasification combined cycle |
| ITR | - Intermediate temperature recuperator |
| LCOE | - Levelized cost of electricity |
| LFG | - Landfill gas |
| LTR | - Low temperature recuperator |
| MAC | - Main air compressor |
| NETL | - National Energy Technology Laboratory |
| NGCC | - Natural gas combined cycle |
| NOAK | - Nth-of-a-kind |
| O&M | - Operation and maintenance |
| PCHE | - Printed circuit heat exchanger |
| QGESS | - Quality Guidelines for Energy System Studies |
| R&D | - Research and development |
| $sCO_2$ | - Supercritical carbon dioxide |
| T&S | - Transport and storage |
| TEA | - Techno-economic analysis |
| TIT | - Turbine inlet temperature |
| TPC | - Total plant cost |

## DISCLAIMER

This project was funded by the Department of Energy, National Energy Technology Laboratory an agency of the United States Government, through a support contract. Neither the United States Government nor any agency thereof, nor any of its employees, nor the support contractor, nor any of their employees, makes any warranty, express or implied, or assumes any legal liability or responsibility for the accuracy, completeness, or usefulness of any information, apparatus, product, or process disclosed, or represents that its use would not infringe privately owned rights. Reference herein to any specific commercial product, process, or service by trade name, trademark, manufacturer, or otherwise does not necessarily constitute or imply its endorsement, recommendation, or favoring by the United States Government or any agency thereof. The views and opinions of authors expressed herein do not necessarily state or reflect those of the United States Government or any agency thereof.

## ACKNOWLEDGEMENTS

The authors would like to thank Travis Shultz (NETL), Richard Dennis (NETL), Can Uysal and Mark Woods (NETL support contractors) for their support and assistance in performing this work.

## REFERENCES

[1] R. Allam, S. Martin, B. Forrest, J. Fetvedt, X. Lu, D. Freed, G. W. Brown Jr, T. Sasaki, M. Itoh and J. Manning, "Demonstration of the Allam Cycle: an update on the development status of a high efficiency supercritical carbon dioxide power process employing full carbon capture," *Energy Procedia,* vol. 114, pp. 5948-5966, 2017.

[2] R. J. Allam, J. E. Fetvedt, B. A. Forrest and D. A. Freed, "The oxy-fuel, supercritical CO2 Allam Cycle: New cycle developments to produce even lower-cost electricity from fossil fuels without atmospheric emissions," in *Turbo Expo: Power for Land, Sea, and Air*, 2014.

[3] R. J. Allam, M. R. Palmer, G. W. Brown Jr, J. Fetvedt, D. Freed, H. Nomoto, M. Itoh, N. Okita and C. Jones Jr, "High efficiency and low cost of electricity generation from fossil fuels while eliminating atmospheric emissions, including carbon dioxide," *Energy Procedia,* vol. 37, pp. 1135-1149, 2013.

[4] International Energy Agency Greenhouse Gas (IEAGHG), "Oxy-Combustion Turbine Power Plants," Cheltenham, United Kingdom, August 2015.

[5] R. Scaccabarozzi, M. Gatti and E. Martelli, "Thermodynamic analysis and numerical optimization of the NET Power oxy-combustion cycle," *Applied energy,* vol. 178, pp. 505-526, 2016.

[6] R. Scaccabarozzi, M. Gatti and E. Martelli, "Thermodynamic optimization and part-load analysis of


DOI: 10.17185/duepublico/77275

the NET Power Cycle," *Energy Procedia,* vol. 114, pp. 551-560, 2017.

[7] A. McClung, K. Brun and J. Delimont, "Comparison of supercritical carbon dioxide cycles for oxy-combustion," in *Turbo Expo: Power for Land, Sea, and Air*, 2015.

[8] C. White and N. Weiland, "Preliminary cost and performance results for a natural gas-fired direct sCO2 power plant," in *The 6th International Supercritical CO2 Power Cycles Symposium*, 2018.

[9] Electric Power Research Institute (EPRI), "Performance and Economic Evaluation of Supercritical CO2 Power Cycle Coal Gasification Plant," (300200374), Palo Alto, California, December, 2014.

[10] R. J. Allam, B. A. Forrest and J. E. Fetvedt, *Method and system for power production with improved efficiency,* Google Patents, 2017.

[11] R. E. James III PhD, D. Kearins, M. Turner, M. Woods, N. Kuehn and A. Zoelle, "Cost and performance baseline for fossil energy plants volume 1: bituminous coal and natural gas to electricity," 2019.

[12] National Energy Technology Laboratory, "Quality Guidelines for Energy System Studies: Specification for Selected Feedstocks," U.S. Department of Energy, Pittsburgh, PA, 2019.

[13] C. W. White and N. T. Weiland, "Evaluation of Property Methods for Modeling Direct-Supercritical CO2 Power Cycles," *Journal of Engineering for Gas Turbines and Power,* vol. 140, p. 011701, 2018.

[14] S. C. Uysal, Analytical Modelling of the Effects of Different Gas Turbine Cooling Techniques on Engine Performance, West Virginia University, 2017.

[15] S. C. Uysal and N. Weiland, "Turbomachinery design of an axial turbine for a direct fired sCO2 cycle," *Energy Conversion and Management,* vol. 267, p. 115913, 2022.

[16] S. C. Uysal, C. W. White, N. Weiland and E. A. Liese, "Cooling analysis of an axial turbine for a direct fired sCO2 cycle and impacts of turbine cooling on cycle performance," *Energy Conversion and Management,* vol. 263, p. 115701, 2022.

[17] R. Le Pierres, D. Southall and S. Osborne, "Impact of mechanical design issues on printed circuit heat exchangers," in *Proceedings of SCO2 Power Cycle Symposium*, 2011.

[18] Y. Jiang, E. Liese, S. E. Zitney and D. Bhattacharyya, "Design and dynamic modeling of printed circuit heat exchangers for supercritical carbon dioxide Brayton power cycles," *Applied Energy,* vol. 231, p. 1019–1032, 2018.

[19] S. Pidaparti, C. W. White, A. C. O'Connell and N. Weiland, "Cooling Technology Models for Indirect sCO2 Cycles," 2020.

[20] K. Gerdes, W. M. Summers and J. Wimer, "Quality Guidelines for Energy System Studies: Cost Estimation Methodology for NETL Assessments of Power Plant Performance," 8 2011.

[21] N. T. Weiland, B. W. Lance and S. R. Pidaparti, "sCO2 Power Cycle Component Cost Correlations From DOE Data Spanning Multiple Scales and Applications," in *ASME Turbo Expo 2019: Turbomachinery Technical Conference and Exposition*, 2019.

[22] National Energy Technology Laboratory, "Quality Guidelines for Energy System Studies: Cost Estimation Methodology for NETL Assessments of Power Plant Performance," U.S. Department of Energy, Pittsburgh, PA, 2019.

[23] T. Grant, "Quality Guidelines for Energy System Studies: Carbon Dioxide Transport and Storage Costs in NETL Studies," 8 2019.

[24] J. C. Eslick, B. Ng, Q. Gao, C. H. Tong, N. V. Sahinidis and D. C. Miller, "A framework for optimization and quantification of uncertainty and sensitivity for developing carbon capture systems," *Energy Procedia,* vol. 63, pp. 1055-1063, 2014.

[25] N. Hansen, S. D. Müller and P. Koumoutsakos, "Reducing the time complexity of the derandomized evolution strategy with covariance matrix adaptation (CMA-ES)," *Evolutionary computation,* vol. 11, pp. 1-18, 2003.

[26] [Online].Available:https://www3.epa.gov/ttncatc1/dir1/landgem-v302-guide.pdf.

[27] [Online].Available:https://www.epa.gov/sites/default/files/2016-12/documents/lfgcost-webv3.1manual_113016.pdf.

[28] G. V. Brigagão, J. L. Medeiros, F. A. Ofélia de Queiroz, H. Mikulčić and N. Duić, "A zero-emission sustainable landfill-gas-to-wire oxyfuel process: Bioenergy with carbon capture and sequestration," *Renewable and Sustainable Energy Reviews,* vol. 138, p. 110686, 2021.

[29] X. Lu, B. Forrest, S. Martin, J. Fetvedt, M. McGroddy and D. Freed, "Integration and optimization of coal gasification systems with a near-zero emissions supercritical carbon dioxide power cycle," in *Turbo Expo: Power for Land, Sea, and Air*, 2016.

[30] X. Lu, "Flexible Integration of the sCO2 Allam Cycle with Coal Gasification Low-Cost Emission-Free Electricity Generation," in *GTC*, 2014.

[31] N. T. Weiland and C. W. White, "Techno-economic analysis of an integrated gasification direct-fired supercritical CO2 power cycle," *Fuel,* vol. 212, pp. 613-625, 2018.


DOI: 10.17185/duepublico/77275

## ANNEX A

| Parameter | Reference NGCC Plants | | Optimized Direct $sCO_2$ Plants | | | |
|---|---|---|---|---|---|---|
| | **B31B.90** | **B31B.97** | **Case A** | **Case B** | **Case C** | **Case D** |
| Gross Power Output (MWe) | 692 | 687 | 793 | 822 | 830 | 836 |
| Auxiliary Power Requirement (MWe) | 47 | 51 | 164 | 180 | 183 | 182 |
| Net Power Output (MWe) | 645 | 637 | 629 | 642 | 647 | 654 |
| Natural Gas Flow Rate (lb/hr) | 205,630 | 205,630 | 205,626 | 205,626 | 205,626 | 205,626 |
| HHV Thermal Input (kWth) | 1,354,905 | 1,354,905 | 1,355,866 | 1,355,866 | 1,355,866 | 1,355,866 |
| Net Plant HHV Efficiency (%) | 47.6% | 47.0% | 46.4% | 47.3% | 47.7% | 48.2% |
| Raw Water Consumption (gpm) | 2,965 | 3,029 | 1,464 | 1,335 | 1,310 | 1,255 |
| $CO_2$ Capture Rate (%) | 90% | 97% | 98.5% | 98.5% | 98.5% | 98.5% |
| $CO_2$ Emissions (lb/MWh-net) | 85 | 26 | 8.9 | 8.8 | 8.7 | 8.6 |
| **Auxiliary Power Breakdown** | | | | | | |
| ASU MAC, kWe | - | - | 84,150 | 100,770 | 100,780 | 100,780 |
| ASU BAC, kWe | - | - | 42,730 | 42,730 | 44,770 | 44,770 |
| Other ASU Auxiliaries, kWe | - | - | 1,000 | 1,000 | 1,000 | 1,000 |
| Natural Gas Compressor Power, kWe | - | - | 13,830 | 13,780 | 13,790 | 13,790 |
| $CO_2$ Capture/Removal Auxiliaries, kWe | 13,600 | 15,200 | - | - | - | - |
| $CO_2$ Compression, kWe | 17,900 | 19,290 | 10,440 | 10,470 | 10,470 | 10,480 |
| Miscellaneous BOP, kWe | 570 | 570 | 570 | 570 | 570 | 570 |
| Combustion/$sCO_2$ Turbine Auxiliaries, kWe | 1,020 | 1,020 | 1,020 | 1,020 | 1,020 | 1,020 |
| Steam Turbine Auxiliaries, kWe | 200 | 200 | - | - | - | - |
| Feedwater Pumps, kWe | 4,830 | 4,830 | - | - | - | - |
| Condensate Pumps, kWe | 170 | 170 | - | - | - | - |
| Circulating Water Pumps, kWe | 4,830 | 4,390 | 1,400 | 1,180 | 1,100 | 1,090 |
| Ground Water Pumps, kWe | 400 | 410 | 160 | 150 | 140 | 140 |
| Cooling Tower Fans, kWe | 2,240 | 2,270 | 740 | 620 | 580 | 570 |
| Adiabatic Cooling System Fans, kWe | - | - | 3,867 | 3,973 | 4,381 | 3,836 |
| Transformer Losses, kWe | 2,220 | 2,210 | 2,760 | 2,890 | 2,920 | 2,940 |
| **Total Auxiliaries, kWe** | **47,492** | **50,562** | **163,917** | **180,403** | **182,771** | **182,236** |

**Table 7:** Performance summary for the optimized direct $sCO_2$ plants and reference NGCC plants

| Parameter | Reference NGCC Plants | | Optimized Direct $sCO_2$ Plants | | | |
|---|---|---|---|---|---|---|
| | **B31B.90** | **B31B.97** | **Case A** | **Case B** | **Case C** | **Case D** |
| Feedwater & Miscellaneous BOP | $113,279 | $113,414 | $71,069 | $69,016 | $68,396 | $67,940 |
| Cryogenic ASU | - | - | $545,498 | $545,497 | $545,522 | $545,522 |
| Flue Gas Cleanup & Piping | $507,564 | $539,258 | $48,756 | $48,813 | $48,313 | $48,832 |
| Combustion/sCO2 Turbine & Accessories | $113,760 | $113,760 | $660,102 | $667,077 | $678,894 | $777,288 |
| HRSG, Ductwork, & Stack | $110,033 | $109,850 | - | - | - | - |
| Steam Turbine & Accessories | $82,513 | $80,986 | - | - | - | - |
| Cooling Water System | $50,697 | $51,068 | $23,398 | $21,040 | $20,128 | $19,989 |
| Accessory Electric Plant | $69,316 | $71,385 | $139,736 | $148,536 | $148,875 | $149,760 |
| Instrumentation & Control | $23,725 | $23,951 | $25,162 | $25,550 | $25,604 | $25,592 |
| Improvements & Site | $28,811 | $28,715 | $30,671 | $31,176 | $31,316 | $31,420 |
| Building & Structure | $18,378 | $18,232 | $8,004 | $8,023 | $8,022 | $8,035 |
| **Total** | **$1,118,075** | **$1,150,619** | **$1,552,386** | **$1,564,728** | **$1,576,569** | **$1,674,377** |
| **Total, $/kWe** | **1,734** | **1,807** | **2,467** | **2,439** | **2,436** | **2,561** |
| **$sCO_2$ Power Cycle Capital Cost Breakdown** | | | | | | |
| Turbine | - | - | $58,724 | $58,724 | $58,724 | $58,724 |
| HTR | - | - | $235,541 | $246,442 | $264,343 | $311,264 |
| ITR | - | - | $42,004 | $43,351 | $41,717 | $45,609 |
| LTR | - | - | $40,798 | $45,757 | $38,476 | $42,980 |
| Water KO Cooler | - | - | $9,235 | $10,149 | $10,785 | $30,810 |
| Pre-compressor | - | - | $56,128 | $56,786 | $56,966 | $56,753 |
| Adiabatic Coolers | - | - | $142,083 | $147,824 | $149,259 | $156,913 |
| Boost Pump | - | - | $16,586 | $16,905 | $16,973 | $17,083 |
| Oxidant/Recycle Compressor | - | - | $17,481 | $17,481 | $17,494 | $31,355 |
| Natural Gas Compressor | - | - | $5,391 | $5,391 | $5,391 | $5,391 |
| Piping | - | - | $5,315 | $5,315 | $5,315 | $5,315 |
| Foundations | - | - | $12,816 | $12,951 | $13,180 | $15,091 |

**Table 8:** Capital cost (TPC/$1,000) summary for the optimized direct $sCO_2$ plants and reference NGCC plants


DOI: 10.17185/duepublico/77275

**DOI:** 10.17185/duepublico/77275
**URN:** urn:nbn:de:hbz:465-20230427-112354-3